

## GAMMA-RAY ASTRONOMY STARTS TO SEE CLAIRE : FIRST LIGHT FOR A CRYSTAL DIFFRACTION TELESCOPE

**H. Halloin<sup>1</sup>, P. von Ballmoos<sup>2</sup>, J. Evrard<sup>3</sup>, G.K. Skinner<sup>2</sup>, J.M. Alvarez<sup>4</sup>, M. Hernanz<sup>4</sup>,  
N.Abrosimov<sup>5</sup>, P.Bastie<sup>6</sup>, B.Hamelin<sup>7</sup>, P. Jean<sup>2</sup>, J. Knödseder<sup>2</sup>, R.K.Smith<sup>8</sup>, and  
G.Vedrenne<sup>2</sup>**

<sup>1</sup>MPI für Extraterrestrische Physik, Postach 1312, Garching, Germany, halloin@mpe.mpg.de

<sup>2</sup>CESR, 9 Av. du Colonel Roche, 31400 Toulouse, France, pvb@cesr.fr

<sup>3</sup>CNES, 18 Avenue Edouard Belin, 31401 Toulouse, France

<sup>4</sup>IIEC, Edifici Nexus, Gran Capità, 2-4, E-08034 Barcelona, Spain

<sup>5</sup>Institut für Kristallzüchtung, 12489 Berlin, Germany

<sup>6</sup>Laboratoire de Spectrométrie Physique, 38402 Saint Martin d'Hères, France

<sup>7</sup>Institut Laue-Langevin, rue des Martyrs, BP 156, 38042 Grenoble, France

<sup>8</sup>ANL, 9700 South Cass Avenue, Argonne, Illinois 60439, USA

### ABSTRACT

CLAIRE is a balloon-borne experiment dedicated to validating the concept of a diffraction gamma-ray lens. This new concept for high energy telescopes is very promising and could significantly increase sensitivity and angular resolution in nuclear astrophysics. CLAIRE's lens consists of 556 Ge-Si crystals, focusing 170 keV gamma-ray photons onto a 3x3 matrix of HPGe detectors, each detector element being only 1.5 x 1.5 x 4.0 cm<sup>3</sup>. On June 14 2001, CLAIRE was launched by the French Space Agency (CNES) from its balloon base at Gap in the French Alps and was recovered near the Atlantic ocean (500 km to the west) after about 5 hours at float altitude. Pointing accuracy allowed for 72 minutes of "good pointing time" on the Crab Nebula. During this time, 33 diffracted photons have been detected leading to a 3 sigma detection of the source. This result, confirmed by other measurements made on the ground (with a radioactive source and a long distance test), validates the concept of diffractive gamma-ray lens for nuclear astrophysics and is the first step towards a space borne instrument.

Key words: gamma-ray astrophysics; diffraction lens; stratospheric flight.

casting (modulating aperture systems such as INTEGRAL and IBIS on board INTEGRAL) or Compton scattering (e.g. COMPTEL on board CGRO). In both these systems, the collecting area is less than or equal to the detecting area. As a consequence, increasing the signal results in increasing the background noise. Thus, building a coded mask telescope ten times better in sensitivity than SPI or IBIS would require to multiply the total weight by a factor of, at least, one hundred, far beyond what could reasonably be launched in space. Besides, the results presented in these proceedings show how important is the complementarity between fine, sensitive spectroscopy (SPI) and good angular resolution (IBIS), in order to precisely localize  $\gamma$ -ray sources and understand their physical properties.

By focusing photons from a large collecting area onto a small detector, a  $\gamma$ -ray lens could achieve both unprecedented sensitivities in the nuclear  $\gamma$ -ray energy range as well as very good angular resolution. Actually, the expected performance of a space borne  $\gamma$ -ray lens (the MAX project) is a sensitivity of a few  $10^{-7}$  ph.s<sup>-1</sup>.cm<sup>-2</sup> in two 100 keV bands centered at 500 and 850 keV (i.e. at least 30 times better than SPI) and a angular resolution of about 1 arcmin, i.e. one order of magnitude lower than the IBIS resolution.

### 1. INTRODUCTION

Due to their high energy, gamma-ray photons penetrating in matter are usually absorbed or incoherently scattered. Thus, focusing techniques was considered as irrelevant for nuclear astrophysics. Actually, present instruments are making use of shadow-

### 2. PRINCIPLES OF A DIFFRACTION LENS

Since the wavelength of  $\gamma$ -ray photons is smaller than distances between atoms in matter, coherently deviating  $\gamma$ -rays was considered as impossible for a long time in nuclear astrophysics and only the corpuscular properties of these photons were used. Nevertheless, Max von Laue, at the beginning of the 20<sup>th</sup>

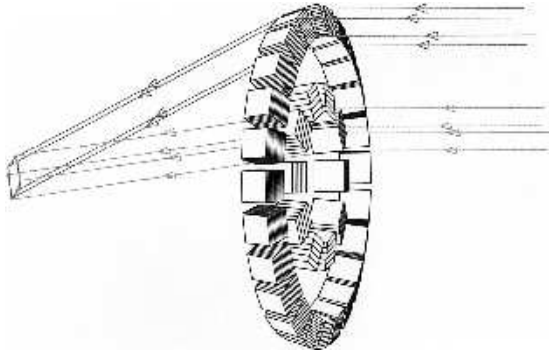


Figure 1. Principle of a gamma-ray lens

century noticed that  $\gamma$ -rays can interact coherently in a crystal lattice, provided that the angles of incident photons are very small and satisfy the Bragg relation :

$$2d \sin \theta = n\lambda, \quad (1)$$

where  $d$  is the crystal plane spacing,  $\theta$  the incident angle with respect to the crystal planes,  $n$  is the reflection order and  $\lambda$  the wavelength of the photon. Thus, by mounting and tuning (i.e. orienting the crystal to get the correct scattering angle  $\theta$ ) adequate crystals on concentric rings, a parallel beam of a given energy can be focused on a single point, provided that the radii of the rings are inversely proportional to the spacing of the diffraction planes. Besides, the high penetrating power of  $\gamma$ -rays and the small angle of incidence (typ. 1 deg) led us choose the so-called Laue geometry. This means that the photon is propagating through the entire crystal, using all the crystal thickness for diffraction (see Fig. 1).

The use of perfect monocrystals is not suitable for a  $\gamma$ -ray lens, since the diffracting angular range (and thus the energy bandwidth) is very narrow (typ. a few arcseconds). Moreover, when the thickness of a perfect crystal is greater than the so-called extinction length (typically from a few tens to a few hundreds of microns for germanium and low energy  $\gamma$ -rays), constructive and destructive interferences are equally generated, so limiting the diffracting power of the crystal. So, in order to improve the efficiency of the lens as well as to increase the field of view of the instrument, “perfectly imperfect” or mosaic crystals are used. These crystals consist of an aggregate of small, perfect crystals. The angular distribution of these crystallites is described by a gaussian function, whose FWHM is called the *mosaic width* or *mosaicity*, i.e. the angular range over which the crystal reflects monochromatic radiation. The mosaicity also defines the field of view of the lens. Such crystals can be produced by adding some impurities in the melted material while the crystal is grown. For the CLAIRE project, germanium crystals with about 1% of silicon were used (Abrosimov 1997). By differentiating the Bragg relation, the energy bandwidth of a  $\gamma$ -ray lens is seen to be proportional to the square

of the diffracted energy :

$$\begin{aligned} \Delta E &\approx \frac{2dE^2 \Delta\theta}{hc} \\ &\approx 40.0 \left( \frac{d}{d_{\text{Ge}[111]}} \right) \left( \frac{E}{511 \text{ keV}} \right)^2 \\ &\times \left( \frac{\Delta\theta}{1 \text{ arcmin}} \right) \text{ keV} \end{aligned} \quad (2)$$

where  $\Delta\theta$  is the *mosaic width* of the crystal. The reflectivity power of mosaic crystals is described by the Darwin model (e.g. Zachariasen 1945).

### 3. TESTING THE CONCEPT OF A $\gamma$ -RAY LENS : THE CLAIRE PROJECT

Based on these principles, the first lens for nuclear astrophysics has been built at the CESR (Toulouse, France) by mounting and tuning germanium-silicon crystals on 8 concentric rings. After having testing the concept of a  $\gamma$ -ray lens (Naya et al. 1996) and the efficiency of Ge(Si) (Kohnle et al. 1998) crystals, the CLAIRE project was dedicating to testing the lens on an astrophysical source.

#### 3.1. Design and tuning of the lens

Since the atmosphere is opaque to the  $\gamma$ -rays, the lens was designed for an observation during a stratospheric flight, which implies a relatively short focal length and an exposure time of typically 3 hours. The diffracted energy was then a trade-off between the effective area, the available focal length and the flux of the astrophysical  $\gamma$ -ray sources. Since no astronomical “standard candle” for  $\gamma$ -ray line emission has been so far discovered, using a section of the continuum emission from the Crab Nebula was an obvious alternative. The lens, constituted of about 560 Ge (physical area of about 511 cm<sup>2</sup> with 0.7x1 and 1x1 cm<sup>2</sup> crystals) was then tuned for a diffracted energy of 170 keV, resulting in a focal length of 2,77 m. The mosaicity of the Ge(Si) between 1 and 2 arcmin led to a field of view of about 1.5 arcmin and a diffracted energy bandwidth of 3 keV. More information about the general design and the objectives of the CLAIRE project can be found in Laporte et al. (2000).

The tuning of the lens consists of tilting each crystal with the right angle so that the diffracting energy is 170 keV for a source placed at infinity, on the optical axis of the lens. According to the Bragg relation and the geometry of the lens, the following formula gives the theoretical relationship between the distance of the source and the diffracted energy :

$$\frac{100 \text{ keV}}{E} = \frac{100 \text{ keV}}{E_\infty} + 0.3251 \left( \frac{10 \text{ m}}{D} \right), \quad (3)$$

where  $E_\infty = 170 \text{ keV}$  is the diffracted energy for a source at infinity. This formula shows that the lens

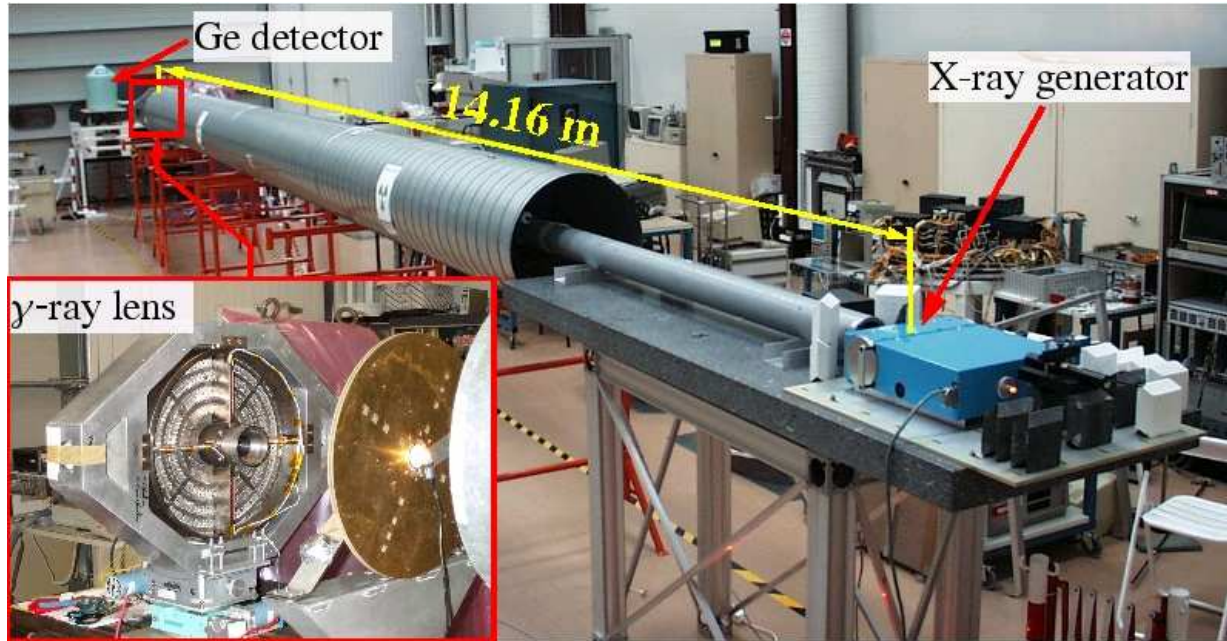


Figure 2. The lens tuning bench at the CESR.

cannot be directly tuned in the laboratory with an energy close to 170 keV, since it would require a source distance of the order of 100 m ! Given the available distance at the CESR (about 20 m), the tuning energy was chosen to 122.28 keV, corresponding to a source distance of 14.16 m (see Fig. 2). The crystals being mounted on small flexible aluminum plates, the tuning method consists of tilting each crystal with a screw, so that the diffracted peak is exactly measured at an energy of 122.28 keV (the required accuracy on the angle is about 10 arcsec).

In order to accurately point the lens at the source, a luminous target is placed immediately in front of the X-ray source. The optical axis of the lens is then defined through the use of a rotating CCD camera mounted in the center of the lens : when looking at an optical source while this telescope is rotated, the image on the CCD describes a circle whose center gives the direction of the rotating axis. This invariant pixel is then used to represent the lens axis. Two rotation stages allow to make the invariant pixel and the light source coincide with an accuracy of a few arcseconds.

The characteristics (shape and flux) of spectra recorded during the tuning allowed the determination of the crystals' parameters (mosaicity and mean length of the crystallites). These parameters were then used for the development of realistic numerical models, which can be compared with experiments in various conditions of pointing, source spectrum and distance, etc.

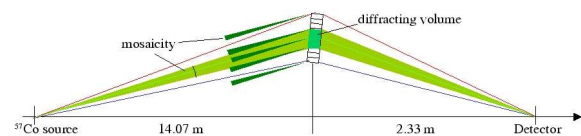


Figure 3. Measurement with a  $^{57}\text{Co}$  source

### 3.2. Other ground based measurements

In order to estimate the diffraction efficiency of the lens, as well as its angular response, two other experiments have been conducted on the ground.

First, a radioactive source of  $^{57}\text{Co}$  was observed with the lens. This source emits a line at 122.06 keV, corresponding to a distance of 14.07 m according to Eq. 3. At this distance, the angular size of each crystal is of 2.4 arcmin (crystal height of 1 cm) or 1.7 arcmin (0.7 cm). Since these values are larger than the mosaicity, only a small fraction of the crystal is diffracting, leading to diffraction efficiency (diffracted fraction of the incident radiation on the lens area) of  $3.2^{\pm 0.1}\%$ . The numerical simulations can then be used to correct this efficiency for a monochromatic, divergent beam into a polychromatic, parallel beam. Finally, taking into account the estimated uncertainties on the crystals' parameters, a semi-empirical value for the peak efficiency at 170 keV (considering an diffracted peak of 3 keV FWHM) can be set to  $7.7^{\pm 1}\%$ .

Additional ground measurements with a source at 205 m were performed on an aerodrome in Figueras, on the Spanish Mediterranean coast. This experiment is described in details in these proceedings (Alvarez et al. 2004), please refer to this article for more

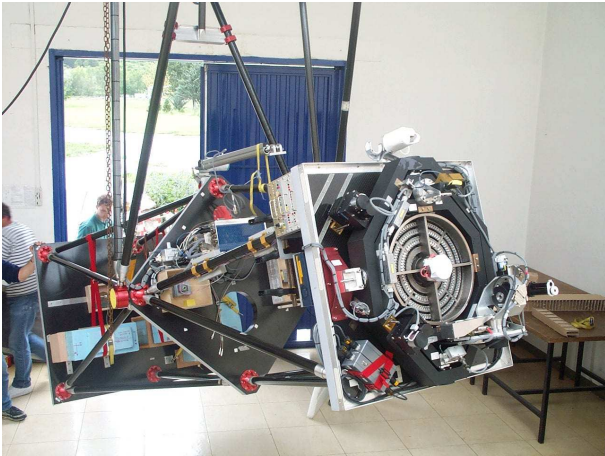


Figure 4. CLAIRe during pointing tests at the launch site.

information. This experiment led to a peak efficiency of  $9.7 \pm 1\%$ , taking into account an estimation of systematic effects. This experiment also validated the theoretical instrumental response of the lens, as well as the pointing procedures.

#### 4. THE CLAIRe 2001 STRATOSPHERIC FLIGHT

On June 14 2001, CLAIRe was launched by the French Space Agency (CNES) from its launch site at Gap in the French Alps and landed near the Atlantic coast 500 km west of the launch site. The float altitude was 41 km and lasted about 5 hours.

##### 4.1. Description of the gondola

The lens module, detector package, and pointing systems were built into a purpose designed telescope structure made of composite materials and weighing about 500 kg (see Fig. 4). The lens and its fine pointing system were held by the upper of three platforms. About 3 meters behind the lens, the lower platform held the detecting system (detector matrix, electronics, collimator, etc.). The  $\gamma$ -ray detector consists of a  $3 \times 3$  HPGe matrix cooled by liquid nitrogen. Each of the 9 elements is a  $1.5 \times 1.5 \times 4$  cm<sup>3</sup> n-type coaxial detector with a central hole 0.5 cm diameter  $\times$  3.5 cm deep. The pointing system was designed to keep the focal spot on the central detector but it can wander around on the Ge matrix as the primary stabilizer seeks its central position. Background noise in Ge detectors usually dominates over the signal in  $\gamma$ -ray astrophysics and is mainly due to secondary emission induced by cosmic rays (e.g. Gehrels 1992). In order to reduce this noise, the matrix was actively shielded by CsI and BGO scintillators. Fig. 5 shows the lens with its fine pointing system (left-hand side) and the Ge-matrix surrounded by the anti-coincidence shield (right-hand side). A detailed description of the fine



Figure 5. Left : CLAIRe's  $\gamma$ -ray lens (diameter 45 cm on the gimbal mount of the fine pointing system). Right : The  $3 \times 3$  HP-Ge matrix surrounded by the anti-coincidence shield.

pointing system and the telescope structure is given in Halloin et al. (2003).

##### 4.2. Performance of the active shield

As previously mentioned, the rejection of the background noise is based on a active anti-coincidence shield (ACS) and on the flagging of some particular events (veto flags) :

- coincidence with the veto gate of the ACS
- occurrence within the resetting time of the electronics (usually after a saturating event)

For the data analysis, all flagged events were strictly rejected. Moreover, only single events were considered (the creation of a multiple event from a diffracted photons is actually very unlikely).

On June 15, 2000, a first, technological, flight was performed with CLAIRe (von Ballmoos et al. 2001) in the same conditions (altitude, trajectory, etc.). During this flight, a technical problem prevented us from correctly pointing the Crab Nebula more than 45'. Nevertheless, it validated the pointing and detection systems. For this maiden flight, the detector was passively shielded with a few millimeters of lead, tantalum and tin. Fig. 6 shows a comparison of background spectra recorded at float altitude for the 2 flights : flight 2000 (passive shielding), flight 2001 without rejecting flagged events, flight 2001 with events rejection. The cutoff at 90 keV for the 2000 flight spectrum is due to the events selection threshold during this flight. The comparison of this spectra with the one recorded in 2001 with ACS turned OFF shows the influence of activation in passive material around the detector : the additional mass required by the ACS produced an higher background (about 50%) than with a light, passive shielding. Nevertheless, when the ACS is turned ON, about 90% of background noise is rejected and only 6 lines are significantly observable in the range from 50 to 800 keV :

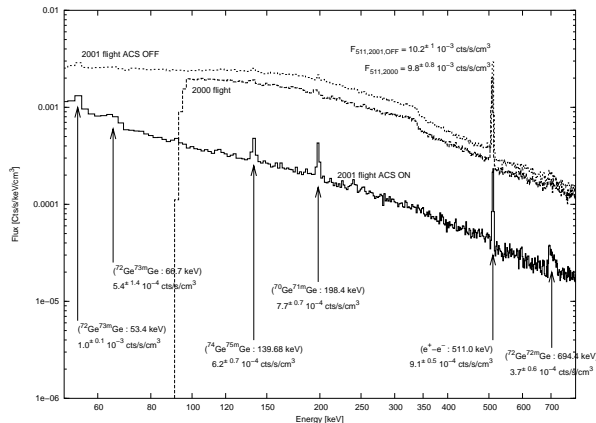


Figure 6. Single events background noise spectra recorded at float altitude during the 2000 and 2001 CLAIRE flights

- Ge  $\beta$  decay lines : 53.4, 66.7, 139.68 and 198.4 keV
- elastic neutron scattering in Ge : 694.4 keV
- $e^+e^-$  annihilation line at 511 keV

Measured flux, live time corrected, for each of these lines is indicated on Fig. 6. Around 170 keV (where the diffracted peak is expected), the continuum background level (all single events at float altitude) is represented with a power law with a spectral index of 1.1 and an amplitude of  $2.1 \cdot 10^{-4}$  cts/s/keV/cm<sup>3</sup> (see Fig. 10).

### 4.3. Pointing performance

A first analysis of CLAIRE's last flight was performed (Halloin et al. 2003) which showed a nominal performance of both pointing and detector systems. Nevertheless the reduced spectrum didn't show any evidence of the Crab emission. The reasons which were eventually identified as responsible have been studied and the results of this investigation is presented in the following paragraphs.

#### 4.3.1. Fine pointing accuracy

The precise knowledge of the pointing of the lens during the flight is crucial for a good discrimination of events. Actually, as seen by Eq. 1, a variation in the pointing results in different diffracted energies for different crystals and thus a broadening (given by Eq. 2) of the detected peak. Given the relatively high background in Ge detectors, the signal becomes rapidly undetectable. This effect was tested during the long distance test (see Alvarez et al. 2004, for details) and was found to be in good agreement with the theoretical predictions. It should be noticed however that the integrated flux remains roughly constant whereas

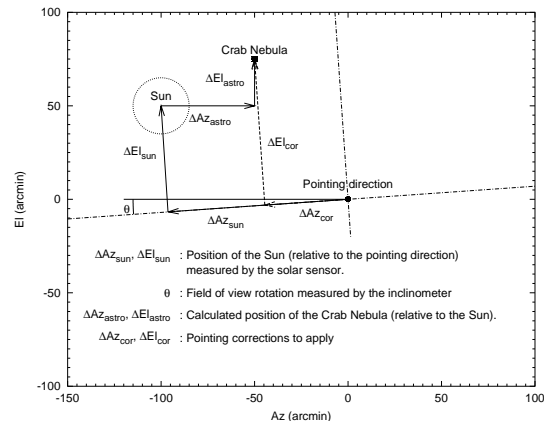


Figure 7. Principle of the fine pointing system. The frame corresponds to the celestial reference, while the dot dashed lines represent the instrument (i.e. CCD camera) axes.

the FWHM of the diffracted peak increases, thus allowing the determination of diffraction efficiency for an assumed perfect pointed experiment (by scaling the peak amplitude to an FWHM of 3 keV).

CLAIRE's stabilization and pointing system was developed by the balloon division of CNES. The sun is used as guide star as it is very close to the Crab Nebula around June 14<sup>th</sup> (about 1 deg). The principle of the fine pointing system is illustrated in Fig. 7.

The pointing method of the lens during the flight is also based on the invariant pixel of the rotating CCD camera (see §3.1). In order to make this invariant pixel and the zero point of the pointing system correspond during the flight, the sun was simultaneously observed by the central telescope and by the solar sensor. Since the same rotating telescope is used to observe a lamp (on the ground) and the sun, an additional density 6 filter was used for the flight. Unfortunately, the prismatic effect of this filter was not properly measured and an offset effect of about 70 arcsec was discovered while the re-processing of the data. Fig. 8 represents the position of the Crab Nebula as seen by the lens during the flight at float altitude corrected for this offset.

Simulations making use of the measured pointing and tuning data show that one should consequently expect the peak at 170 keV to be broadened to 8 keV FWHM.

#### 4.3.2. Primary pointing accuracy

While, the fine pointing system is dedicated to orientating the lens axis towards the Crab Nebula, the position of the focal spot on the detector matrix depends on a separate, primary, pointing system. This system is designed to stabilize and point the entire telescope in order to keep the detector aligned with the lens. To keep the focal spot on the matrix or



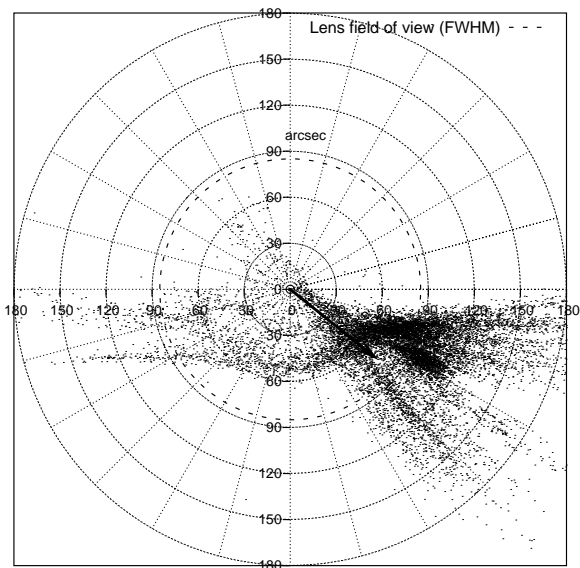


Figure 8. Position of the Crab Nebula as seen by the lens at float altitude. The lens axis is at the center of the graph. The arrow represents the contribution due to the prismatic effect of the solar filter. Each point is the mean value over 1 s.

on the central detector requires a primary pointing accuracy of  $\pm 28$  and  $\pm 9$  arcminutes, respectively.

As mentioned in Halloin et al. (2003), direct use of the fine pointing data did not show any evidence of a peak at 170 keV in the flight spectrum. We then suspected a shift of the focal point with respect to the detector. After the reassembling of the telescope structure, comparison of measurements in the orientation typically used during the observations (elevation of about 60 deg) and in the vertical position (used for detector centering) demonstrated that the focal point moved by 4.5 to 6 mm on the vertical axis and between -15 and 15 mm on the horizontal axis.

#### 4.3.3. Crab detection

As simulation predicts a detected 8 keV FWHM peak at 170 keV, several data analysis were performed with these parameters held fixed while detector offsets were chosen in the mechanically admissible area. 60 trials were made with supposed offsets of 5 and 6 mm along the vertical axis and with a 1 mm step scan between -15 and 15 mm along the horizontal axis. The maximum significance during this “fishing expedition” was found with a  $3.5 \sigma$  (probability of 99.976 %) detection and assuming offsets of +5 mm in the vertical and +10 mm in the horizontal directions. Fig. 9 is a cumulative 2D-histogram on the detector during Crab pointing after correction of these detector offsets. Due to the imperfect stability of the azimuthal axis, the focal point was oscillating from the right (detector 4) to the left (detector 6) with a period of about 170 s. The spectrum corresponding to the maximum sig-

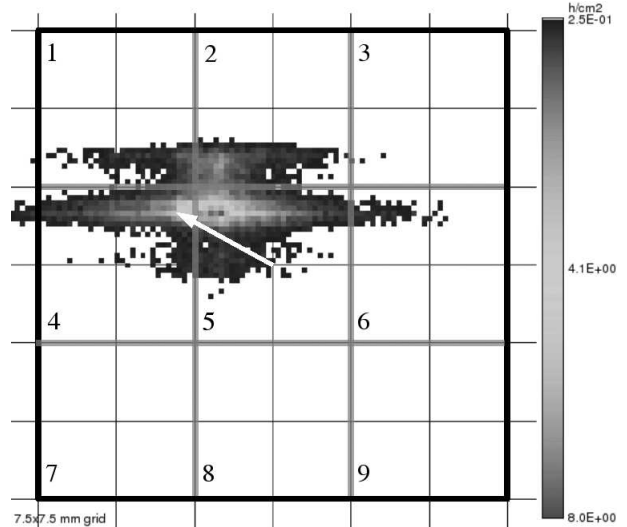


Figure 9. Position of the center of the focal point on the 3x3 Ge matrix during Crab pointing. The arrow shows the displacement of the focal point due to mechanical offsets.

nificance of the search for the detector offsets is plotted in Fig. 11. This spectrum shows a significant excess of about 33 photons at 170 keV with an exposure time of 1<sup>h</sup>12. As a comparison, a spectrum of all single events for every detector at float altitude (reference for background) is shown in Fig. 10. The higher level of continuum in the background spectrum is mainly due to different background levels in different detectors and to their temporal variability.

The number of trials necessary to find this  $3.5 \sigma$  detection (the search for the detector offsets) should be taken into account. In other words, one should estimate the probability of having a detection greater than  $3.5 \sigma$  with background noise only and using the same procedure as previously explained (the 60 trials). Actually, the 60 different positions are strongly interdependent since spectra deduced from adjacent positions contain a large number of common events. The probability distribution of “false” detection cannot be easily calculated since it depends (at least) on background noise levels, common good pointing time between different positions, fitting procedures, etc. Nevertheless this probability distribution can be estimated through Monte-Carlo simulations. Knowing the background noise spectrum for each detector during the flight and the respective exposure time for each position of the “fishing expedition”, numerous searches on the 60 offsets positions for a positive detection on synthetic data (containing no source !) were performed. For each of these searches the maximum detection is retained and used to estimate the probability of the highest detection be less than  $n \sigma$ . Fig 12 shows the results of 625 simulations. The probability distribution is very well fitted by a normal distribution with a mean of  $2 \sigma$  and a standard deviation of 0.47. According to this fit the probability of finding a highest detection less than  $3.5 \sigma$  while analyzing the 60 different data sets of synthetic

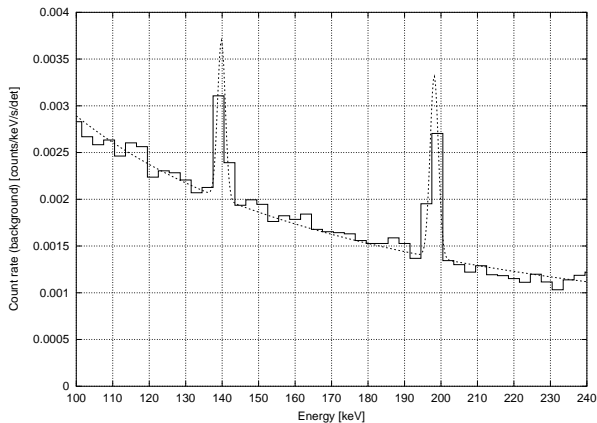


Figure 10. Spectrum for single events at float altitude (background noise spectrum)

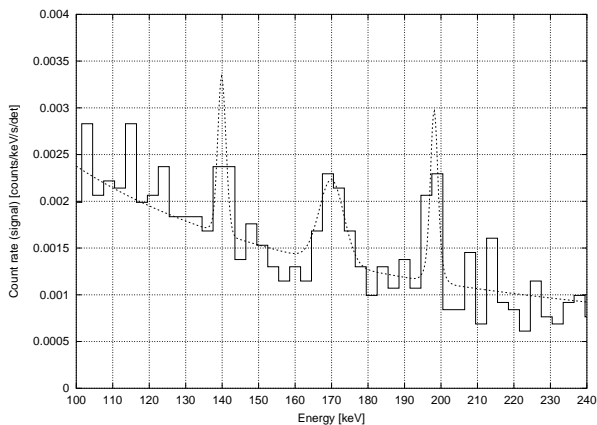


Figure 11. Reduced spectrum for single events and good pointing time intervals

background is 99.898 %. This figure is then also the corrected detection confidence level. It corresponds to a (single trial) result at the  $3\sigma$  level. This also implies that the 60 dependent trials are equivalent to about 4.2 independent trials ( $0.99976^{4.2} \approx 0.99898$ ).

In order to deduce the diffraction efficiency of the lens, one should also calculate the atmospheric absorption as well as the detector efficiency during the “good time intervals” used for the events selection. These values were obtained through Monte-Carlo simulations of the flight, using a GEANT3 simulation of the detector matrix and the U.S standard atmosphere (1976) for the atmosphere modelisation. 1000 simulated flights led to a mean atmospheric transmission of 67% and a detector efficiency of 45.5%. This latter result is noticeably lower than the mean efficiency for a homogeneous illuminated detector, since the focal spot was mainly on the edge of the central detector (see Fig. 9), where the detection efficiency is lower.

Besides, the livetime of the acquisition system (fraction of exposure time available for data acquisition) is estimated to 85%.

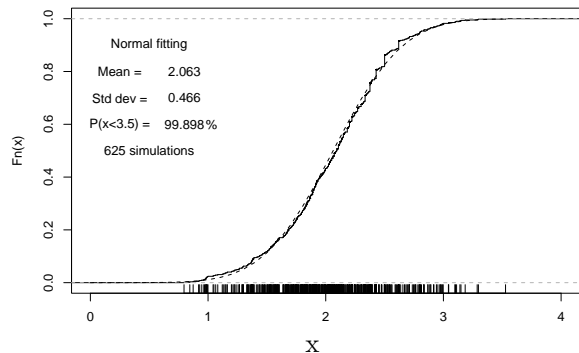


Figure 12. The simulated and fitted probability distribution of false detections in the search for detector offsets.  $F_n(x)$  is the probability observed during the simulations with synthetic background that the most significant point among 60 trials is less than  $x\sigma$ .

Finally, given the Crab nebula flux of  $1.42^{+0.02}_{-0.01} \cdot 10^{-4}$  phot/s/cm<sup>2</sup>/keV at 170 keV (Bartlett 1994), the 33 detected photons leads to a peak efficiency of  $12.5^{+4}\%$ , corrected for a perfect pointing (3 keV FWHM diffracted peak). Due to the method used for the determination of the mechanical detector offsets (maximization of detection likelihood), this value is probably overestimated. This systematic effect is difficult to evaluate and a conservative efficiency value of 10% seems more realistic.

## 5. CONCLUSION

The first crystal diffraction lens diffraction lens has been developed at the CESR and then tested on the ground and with an observation of the Crab Nebula during a balloon flight. Moreover, the measurements performed while tuning the lens allows the comparison of these experiments with numerical simulations (see Table 1). Measurements and simulations are in good agreement and a conservative value of  $9^{+1}\%$  of diffraction efficiency for a polychromatic source at infinity is compatible with experimental and simulated results. One should also notice that, according to the tuning data, some crystals are much more efficient than others. Thus, by carefully selecting only the more efficient crystals, the  $\gamma$ -ray lens efficiency could be increased by a factor of at least 2.

Besides, the validity of the relationship between distance and diffracted energy (Eq. 3) have been tested with various experiments using a continuum source :

- tuning data (distance of 14.16 m)
- source at 22.52 m with a partially tuned lens
- long distance test (205 m)

Experiment	Measured eff. <sup>a,b</sup>	Simulated eff. <sup>a,c</sup>	Comments
Polychromatic source at infinity	$12.5^{+4}_{-2}$ %	$8.88^{\pm 0.02}$ %	Measurement derived from the 2001 flight analysis
Polychromatic source at 205 m	$9.7^{\pm 0.3 \pm 1}$ %	$8.53^{\pm 0.02}$ %	Long distance test (see Alvarez et al. 2004)
<sup>57</sup> Co at 14 m	$3.17^{\pm 0.02 \pm 0.1}$ %	$3.668^{\pm 0.004}$ %	Laboratory experiment with a radioactive source

<sup>a</sup> Peak efficiency assuming a peak FWHM of 3 keV for polychromatic sources, diffracted fraction of the incident flux on the lens for monochromatic sources.  
<sup>b</sup> Error bars include the statistical uncertainty (first figure) and an estimation of systematic effects (second figure).  
<sup>c</sup> Error bars are only statistical.

Table 1. Comparison of experimental results and simulations

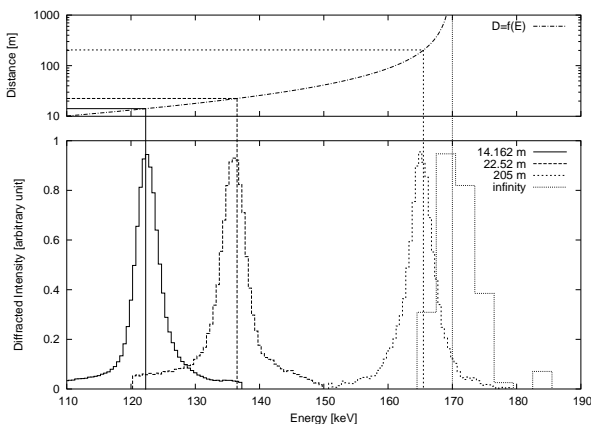


Figure 13. Recorded spectra for continuum sources at various distances.

- stratospheric flight (infinity...)

Fig. 13 represents the recorded spectra for these experiments (lower graph), compared with the theoretical relationship given by Eq.3 (upper graph). The position of the centroids are in very good agreement with theory, slight departures from theoretical values (less than 0.5 keV) being the consequence of the incident spectrum shape and/or the detector calibration drifts.

CLAIRE's stratospheric flight was the first observation of an astrophysical source with a  $\gamma$ -ray lens. Associated with ground measurements and numerical simulations, these results validate the concept of a  $\gamma$ -ray lens for nuclear astrophysics. CLAIRE is the first step in the development of diffraction  $\gamma$ -ray lenses. Ultimately, a space-borne instrument, with longer exposure time and steady pointing, would provide unprecedented angular resolution in the astrophysical  $\gamma$ -ray field (1 arcmin) and outstanding narrow line sensitivities (a few  $10^{-7}$  ph.s<sup>-1</sup>.cm<sup>-2</sup> in two 100 keV bands centered at 500 and 850 keV). This project, called MAX, is the subject of another article in these proceedings (von Ballmoos et al. 2004).

## ACKNOWLEDGMENTS

The authors wish to thank the French Space Agency (CNES), which has built the pointing system and operated the flight from the launch to the gondola recovery. This work was also supported by the U.S. Department of Energy, Basic Energy Sciences, under contract n° W-31-109-Eng-38.

## REFERENCES

- Abrosimov N.V., 1997, J. Crystal Growth, 166, 657  
Alvarez J.M., Halloin H., Hernanz M., et al., 2004, In: ESA SP-552: Proceedings of the 5<sup>th</sup> INTEGRAL Science Workshop, this volume  
Bartlett L.M., 1994, High Resolution Gamma-Ray Spectroscopy of the Crab, Ph.D. thesis, University of Maryland  
Gehrels N., 1992, Nuclear Instruments and Methods in Physics Research, Sect. A, 313, 513  
Halloin H., von Ballmoos P., Evrard J., et al., 2003, Nuclear Instruments and Methods in Physics Research, Sect. A, 504, 120  
Kohnle A., Smither R., Graber T., et al., 1998, Nuclear Instruments and Methods in Physics Research, Sect. A, 408, 553  
Laporte P., Abrosimov N.V., Bastie P., et al., 2000, Nuclear Instruments and Methods in Physics Research, Sect. A, 442, 438  
Naya J.E., von Ballmoos P., Smither R.K., et al., 1996, Nuclear Instruments and Methods in Physics Research, Sect. A, 373, 159  
von Ballmoos P., Evrard J., Skinner G.K., et al., 2001, In: ESA SP-459: Proceedings of the 4<sup>th</sup> INTEGRAL Workshop 'Exploring the Gamma-Ray Universe', 649-652  
von Ballmoos P., Halloin H., Skinner G., et al., 2004, In: ESA SP-552: Proceedings of the 5<sup>th</sup> INTEGRAL Science Workshop, this volume  
Zachariasen W.H., 1945, Theory of X-Ray Diffraction in Crystals, Dover Publications Inc., New York